Phase formation and thermoelectric properties of $Zn_{1+x}Sb$ binary system

Ahmad OSTOVARI MOGHADDAM[1], Evgeny TROFIMOV[1], Ting ZHANG[2], Jordi ARBIOL[2], Andreu CABOT[3,4]

1. Department of Materials Science, Physical and Chemical Properties of Materials,
South Ural State University, 76 Lenin Ave, Chelyabinsk, 454080, Russia;
2. Catalan Institute of Nanoscience and Nanotechnology (ICN2),
Consejo Superior de Investigaciones Científicas (CSIC) and Barcelona Institute of Science and Technology (BIST),
Campus Autonomous University of Barcelona (UAB), Bellaterra, 08193 Barcelona, Spain;
3. Catalonia Institute for Energy Research-IREC, Sant Adrià de Besòs, 08930 Barcelona, Spain;
4. Catalan Institution for Research and Advanced Studies-ICREA, Pg. Lluís Companys 23, 08010 Barcelona, Spain

Abstract: The phase formation and thermoelectric (TE) properties in the central region of the Zn−Sb phase diagram were analyzed through synthesizing a series of $Zn_{1+x}Sb$ (x=0, 0.05, 0.1, 0.15, 0.25, 0.3) materials by reacting Zn and Sb powders below the solidus line of the Zn−Sb binary phase diagram followed by furnace cooling. In this process, the nonstoichiometric powder blend crystallized in a combination of ZnSb and β-Zn_4Sb_3 phases. Then, the materials were ground and hot pressed to form dense ZnSb/β-Zn_4Sb_3 composites. No traces of Sb and Zn elements or other phases were revealed by X-ray diffraction, high resolution transmission electron microscopy and electron energy loss spectroscopy analyses. The thermoelectric properties of all materials could be rationalized as a combination of the thermoelectric behavior of ZnSb and β-Zn_4Sb_3 phases, which were dominated by the main phase in each sample. $Zn_{1.3}Sb$ composite exhibited the best thermoelectric performance. It was also found that Ge doping substantially increased the Seebeck coefficient of $Zn_{1.3}Sb$ and led to significantly higher power factor, up to 1.51 $mW \cdot m^{-1} \cdot K^{-2}$ at 540 K. Overall, an exceptional and stable TE figure of merit (Z_T) of 1.17 at 650 K was obtained for $Zn_{1.28}Ge_{0.02}Sb$.
Key words: $Zn_{1+x}Sb$; ZnSb/β-Zn_4Sb_3 composite; thermal stability; thermoelectric properties

1 Introduction

The design and engineering of thermoelectric (TE) materials are fascinating research areas due to the huge economic and social implications of the direct conversion of heat into electricity and vice versa. Although, TE modules are relatively simple and reliable, as they contain no fluids or moving parts, their efficiency needs to be improved and their cost should be reduced to become cost-effective for widespread potential application [1,2]. The efficiency of a TE module can be estimated by a material figure of merit, $Z_T=S^2\sigma T/k$, where S is the

Seebeck coefficient, σ is the electrical conductivity, k is the thermal conductivity and T is the thermodynamic temperature [3−5].

Among the known TE materials, the binary Zn−Sb system provides several environmental friendly and relatively low cost phases with excellent TE properties in the intermediate temperatures range (473−673 K). Zn−Sb materials could replace current thermoelectric materials operating in this temperature range that generally contain rare and toxic elements, such as Te and Pb [6]. Among different Zn−Sb phases, the two with the highest potential are ZnSb and β-Zn_4Sb_3.

β-Zn_4Sb_3 crystallizes in a hexagonal crystal

structure ($R\overline{3}c$ space group) consisting of 6 Sb_2^{4-} dimers, 18 isolated Sb^{3-} and 39 Zn^{2+} cations [7]. This complex structure provides β-Zn_4Sb_3 with an ultra-low thermal conductivity and an outstanding TE figure of merit Z_T=1.4 at 748 K [8]. However, thermal instability is a well-known concern in all β-Zn_4Sb_3 TE compounds, which has hindered their practical applications [9,10]. β-Zn_4Sb_3 shows two polymorphic phase transitions. It undergoes a transition to disordered α phase below 263 K and transforms to γ-Zn_4Sb_3 above 765 K [6]. More importantly, degradation in β-Zn_4Sb_3 begins at temperatures below the anticipated transition temperature (765 K) due to Zn loss and the subsequent formation of ZnSb and Zn phases as partial inclusions [11]. Furthermore, there are some reports on the decomposition of β-Zn_4Sb_3 to ZnSb and Zn even below 500 K [12].

On the other hand, ZnSb shows suitable thermal stability over the temperature range of 300−850 K. In comparison with β-Zn_4Sb_3, ZnSb possesses higher electrical resistivity and larger Seebeck coefficient [13−15]. Nevertheless, its high thermal conductivity leads to relatively low TE performance with a maximum Z_T around 0.6 at 550 K [16]. A common route to decrease thermal conductivity is through introducing phonon scattering centers at different lengths scales such as point, line and planar lattice defects, grain boundaries, embedded nanodomains and secondary phases. In our previous study, we demonstrated the potential of using ZnSb/Zn_4Sb_3 interfaces to promote the phonon scattering and reached a Z_T value of 1.2 in Ge-doped ZnSb/β-Zn_4Sb_3 nano-composites [6].

In spite of the numerous publications on Zn−Sb materials, there is still a lack of knowledge on the phase formation and TE properties in the central region of the Zn−Sb phase diagram between ZnSb and Zn_4Sb_3 compositions, i.e. around $Zn_{1.3}Sb$. After further and thorough study of this system, we realized that small off-stoichiometries in the Zn−Sb binary system systematically resulted in the simultaneous formation of β-Zn_4Sb_3 and ZnSb phases. Additionally, the β-Zn_4Sb_3 decomposition also occurs during the thermal cycles to which the material is exposed in working conditions. Thus, we believe that it is of particular scientific and technological importance to examine the TE properties of materials containing both phases,

ZnSb and β-Zn_4Sb_3.

In the present work, a series of $Zn_{1+x}Sb$ (x=0, 0.05, 0.1, 0.15, 0.25, 0.3) materials were synthesized by solid state reaction of precursor powders followed by furnace cooling at a low rate near to thermodynamic equilibrium. In contrast to the conventional synthesis routes of β-Zn_4Sb_3 that typically employ a high temperature of about 904 K, the melting point of Sb (or more routinely of about 1023 °C to speed up the reaction), followed by quenching to room temperature [17], we used a significantly lower temperature of 800 K followed by low rate furnace cooling to hinder the formation of unstable phases. The Zn−Sb phases formed in this process and their TE properties were thoroughly investigated.

2 Experimental

$Zn_{1+x}Sb$ (x=0, 0.05, 0.1, 0.15, 0.25, 0.3) materials were synthesized by standard high temperature reaction of the elemental powders mixture. High purity Sb (99.5%, Alfa-Aesar) and Zn (99.9%, Alfa-Aesar) elemental powders in the appropriate ratio were weighed and placed into quartz ampoules. The handling of powders was carried out under argon atmosphere inside a glove box. The filled ampoules were then slowly evacuated and filled with nitrogen for three times and finally sealed under a vacuum of about 1.33×10^{-2} Pa. The sealed ampoules were placed vertically inside a furnace, heated to 800 K at a rate of 100 K/h and soaked for 18 h at that temperature. The furnace was subsequently turned off and the ampoules were allowed to cool down to ambient temperature inside the furnace. The ampoules were broken and the out-coming samples were ground in an agate mortar inside the glove box. The obtained powders were loaded into 8 mm-diameter graphite dies and uniaxiallly hot pressed at 673 K and 100 MPa for 5 min, under Ar atmosphere. The obtained pellets were then annealed at 653 K for 1 h under Ar atmosphere. The relative densities of all the consolidated samples in this study were ~95% of the theoretical value, as measured by Archimedes' method. Besides, to optimize TE properties of the non-stoichiometric $Zn_{1+x}Sb$ samples, Ge-doped $Zn_{1.28}Ge_{0.02}Sb$ sample was also produced using exactly the same procedure detailed above.

X-ray diffraction (XRD) analysis of the hot-

pressed samples was carried out on a Bruker AXS D8 ADVANCE X-ray diffractometer using Cu K$_{\alpha}$ radiation (λ=0.15406 Å) with a scan rate of 5 s per step and step size of 0.01°. Rietveld refinements were performed using the GSAS-II package for quantitative phase analysis [18]. The morphology and elemental analysis of the samples were examined using a scanning electron microscope (SEM, Zeiss Auriga) equipped with an energy dispersive X-ray spectroscopy (EDS) detector (Oxford Instruments). High resolution transmission electron microscopy (HRTEM) and scanning transmission electron microscopy (STEM) studies were performed on a field emission gun FEI Tecnai F20 microscope at 200 kV with a point-to-point resolution of 0.19 nm. High angle annular dark-field (HAADF)-STEM was combined with EELS in the Tecnai microscope by using a GATAN QUANTUM filter.

Seebeck coefficient and electrical resistivity were measured simultaneously during the sample heating up cycle over the temperature range of 300−650 K in a LSR−3 LINSEIS system under helium atmosphere. Thermal conductivity was calculated as a product of thermal diffusivity (λ), heat capacity (c_p) and mass density (ρ') of the samples ($k=\lambda\cdot\rho'\cdot c_p$). Thermal diffusivity was measured using XFA 600 Xenon Flash apparatus. The specific heat (c_p) and the density were estimated using Dulong−Petit approximation and Archimedes' method, respectively.

3 Results and discussion

3.1 Crystallographic phase

The XRD spectra of hot-pressed Zn$_{1+x}$Sb (x=0, 0.05, 0.1, 15, 0.25, 0.3) samples are shown in Fig. 1. A pure ZnSb phase (JCPDS card 96-900-8883) with no traces of un-reacted Zn and Sb elements nor of β-Zn$_4$Sb$_3$ (JCPDS card 96-400-1475) was obtained for x=0. Using an excess of Zn, the β-Zn$_4$Sb$_3$ phase appeared and its fraction increased with increasing x in Zn$_{1+x}$Sb. At x=0.15, nearly the same amount of both ZnSb and β-Zn$_4$Sb$_3$ phases was detected. Further increasing x up to 0.3 did not allow producing pure β-Zn$_4$Sb$_3$ owing to the relatively low synthesis (reaction) temperature, and even at x=0.3, the synthesized samples contained minor amount of ZnSb. For all other samples, the XRD spectra were consistent with a pure mixture of ZnSb

and β-Zn$_4$Sb$_3$ phases, without unreacted Zn and Sb elements. Quantitatively, the amount of β-Zn$_4$Sb$_3$ phase increased from 0 to 11.6%, 38.9%, 49.8%, 77.1% and 85.6% in samples with x=0, 0.05, 0.1, 0.15, 0.25 and 0.3, respectively, as determined by quantitative Rietveld analyses.
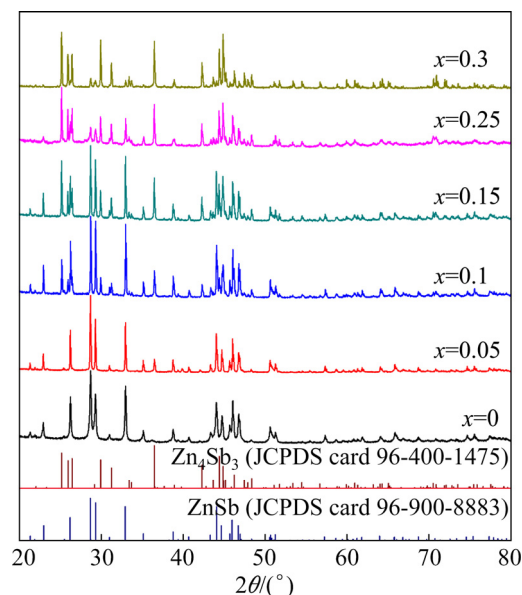

Fig. 1 XRD patterns of Zn$_{1+x}$Sb materials for different values of x

It has been previously reported that a pure β-Zn$_4$Sb$_3$ phase could be obtained when the Zn to Sb ratio falls between 1.3 and 1.33 [19]. If the Zn content is higher than 1.33%, there will not be enough lattice interstitial sites for all the Zn atoms, resulting in the precipitation of Zn or the formation of ZnSb depending on the amount of Sb atoms present in the initial composition. BALASUBRAMANIAN et al [20] found that in a Co-doped Co$_{0.05}$Zn$_{3.95}$Sb$_3$ sample, various combinations of the secondary phases such as ZnSb, Zn and Sb formed in different processing routes. They attributed this observation to the lack of a sufficient amount of Zn to form single phase of Zn$_4$Sb$_3$. However, we detected a combination of ZnSb and β-Zn$_4$Sb$_3$ phases for all Zn$_{1+x}$Sb samples even at Zn content lower than 1.3%, and the fraction of β-Zn$_4$Sb$_3$ phase increased with increasing x in Zn$_{1+x}$Sb. ZHANG et al [21] also obtained a combination of ZnSb and β-Zn$_4$Sb$_3$ phases when the starting compositions were Zn$_{56}$Sb$_{44}$, Zn$_{57}$Sb$_{43}$ and Zn$_{58.5}$Sb$_{41.5}$. Recently, LO et al [17] reported that pure Zn$_{13-\delta}$Sb$_{10}$ (or Zn$_4$Sb$_3$)

phase can be synthesized with the Zn to Sb ratio of 1.3, and there is no need to use a Zn-richer ratio of 1.33 (Zn_4Sb_3 composition). They also obtained materials containing both ZnSb and β-Zn_4Sb_3 phases at room temperature in samples with the starting composition of Zn_9Sb_7, $Zn_{12.7}Sb_{10}$ and $Zn_{12.8}Sb_{10}$. However, our study revealed that not only ZnSb forms as the second phase in β-Zn_4Sb_3 matrix when the starting composition is Zn-deficient $Zn_{1.3-\delta}Sb$, but also the β-Zn_4Sb_3 secondary phase precipitates in a ZnSb matrix when the starting composition is Zn-rich $Zn_{1+\delta}Sb$. Besides, it should be also noted that we used a synthesis temperature of 800 K, where both ZnSb and β-Zn_4Sb_3 phases are in solid state. We believe that synthesizing below solidus temperatures followed by slow cooling results in materials with a superior thermal stability compared to high-temperature synthesis followed by quenching.

3.2 Microstructural characterization

The microstructural morphologies of $Zn_{1+x}Sb$ (x=0.3) sample and the EDS spectrum of the outlined area are shown in Fig. 2(a). Quantitative EDS results are presented in Table 1. A typical morphology of solidified samples, coarse grains with unclear interfaces, was observed in the fracture surface of hot-pressed $Zn_{1.3}Sb$ sample. Identical morphological characteristics were also observed for all the other samples. The results of EDS analysis indicated a uniform distribution of Zn and Sb elements with no significant segregation on the
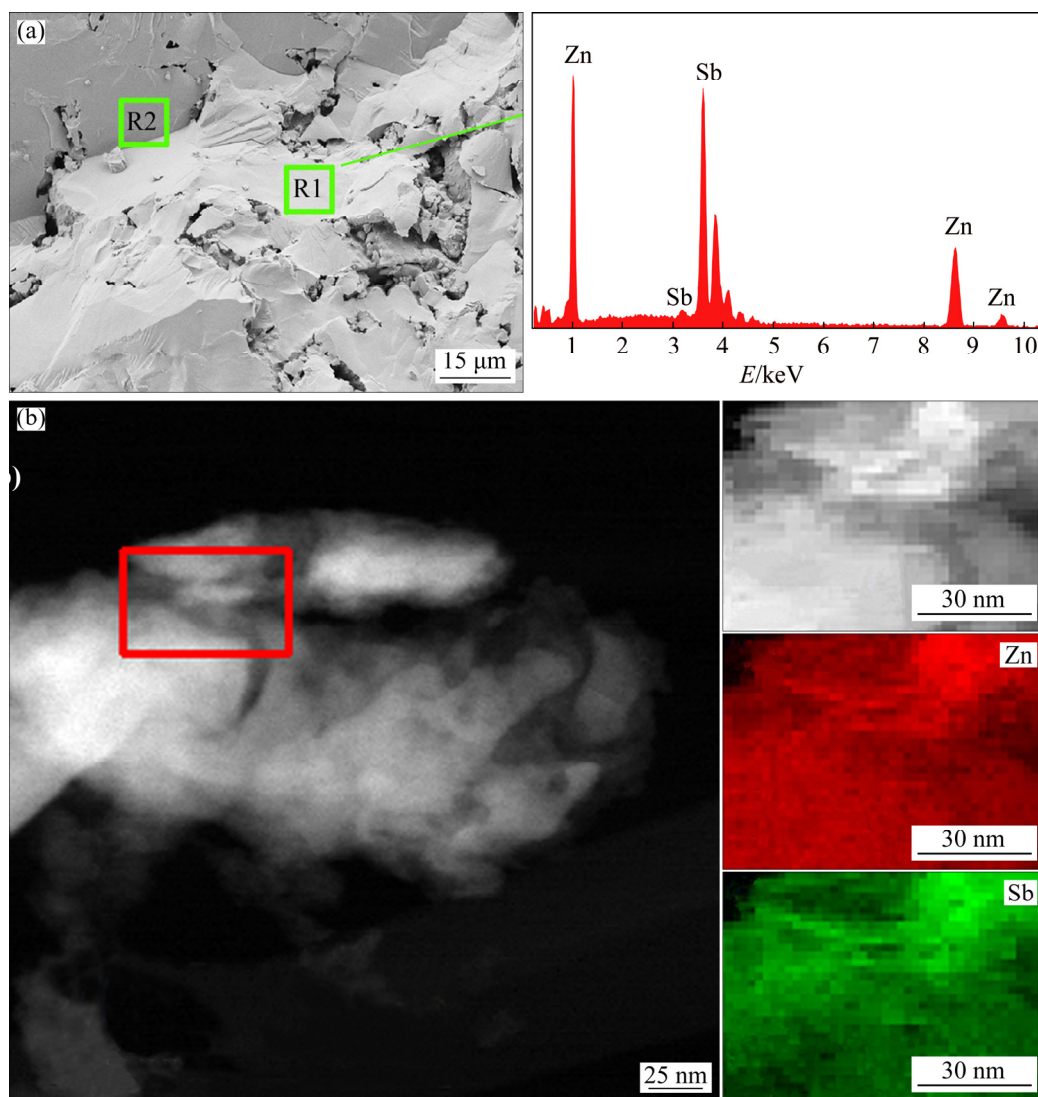

Fig. 2 SEM image of fracture surface of $Zn_{1.3}Sb$ sample and corresponding EDS spectrum of outlined region (a), and EELS chemical composition maps obtained from red squared area of STEM micrograph of $Zn_{1.1}Sb$ sample (Individual Zn L2,3-edges at 1020 eV (red), and Sb M4,5-edges at 528 eV (green)) (b)

Table 1 EDS analysis results of regions outlined in Fig. 2

Element	R1		R2	
	wt.%	at.%	wt.%	at.%
Zn	41.93	56.35	39.95	56.45
Sb	58.07	43.65	60.05	43.55

Average chemical composition: $Zn_{1.29}Sb$

microscopic scale. A slight Zn deficiency was observed for all samples, which may be ascribed to the p-type conductivity of all $Zn_{1+x}Sb$ samples. However, the average EDS results were very close to the compositions of starting powders. The elemental distribution within the $Zn_{1+x}Sb$ samples was further examined by HAADF-STEM characterization and EELS chemical composition maps (Fig. 2(b)). EELS elemental maps confirmed the homogenous distribution of Zn and Sb all through each crystal domain. The results suggested that non-stoichiometric $Zn_{1+x}Sb$ materials with uniform chemical distribution could be synthesized at relatively lower temperatures than those reported in the literatures [17,22,23].

The high-resolution TEM (HRTEM) images of $Zn_{1+x}Sb$ ($x=0.1$) sample are shown in Fig. 3. A thorough power spectrum analysis of the HRTEM micrograph revealed two different crystallographic domains of ZnSb and Zn_4Sb_3 phases. For both rectangular areas in Fig. 3, the crystal structure was found to match the orthorhombic ZnSb phase visualized along different zone axes. The power spectrum of Area R1 disclosed the crystal structure to be consistent with the orthorhombic ZnSb phase (space group: *Pbca*) with $a=6.2016$ Å, $b=7.7416$ Å and $c=8.0995$ Å. Besides, the ZnSb lattice fringe distances were measured to be 0.169, 0.193 and 0.280 nm, at 45.26° and 80.65°, which was interpreted as the orthorhombic ZnSb phase (space group: *Pbca*), visualized along its [215] zone axis. For the Area R2, the lattice fringe distances were ascertained to be 0.337, 0.192 and 0.279 nm, at 45.11° and 79.98°, which could be interpreted as the orthorhombic ZnSb phase visualized along its $[\overline{2}5\overline{1}]$ zone axis. A detailed comparison between the theoretical and experimental bulk plane distances and angles is shown in Table 2. Extensive
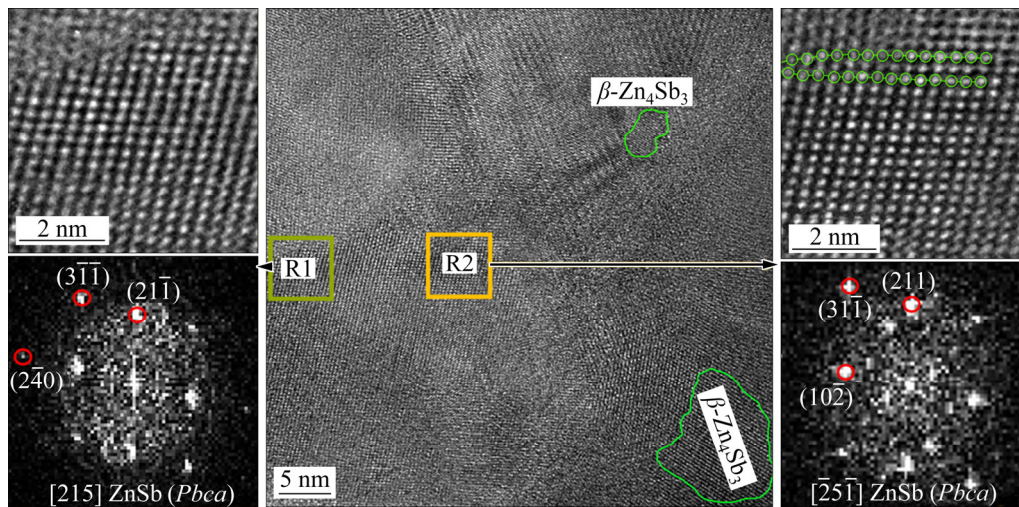

Fig. 3 HRTEM micrograph of consolidated $Zn_{1.1}Sb$ sample showing both ZnSb and β-Zn_4Sb_3 phases (Green-circled areas show β-Zn_4Sb_3 domains; Enlarged images from green and yellow rectangular areas and corresponding power spectrum are also shown, interpreted as orthorhombic ZnSb phase (space group: *Pbca*), visualized along its [215] and $[\overline{2}5\overline{1}]$ zone axes, respectively)

Table 2 Comparison between experimental and theoretical bulk plane spacing distances and angles between planes

Spot	R1		R2	
	Experimental/nm	[215] ZnSb (*Pbca*)/nm	Experimental/nm	$[\overline{2}5\overline{1}]$ ZnSb (*Pbca*)/nm
1	0.169	0.164 $(2\overline{4}0)$	0.337	0.339 $(20\overline{4})$
2	0.193 (45.26° vs Spot 1)	0.194 (44.83°) $(3\overline{1}\overline{1})$	0.192 (45.11° vs Spot 1)	0.194 (44.49°) $(31\overline{1})$
3	0.280 (80.65° vs Spot 1)	0.271 (80.45°) $(21\overline{1})$	0.279 (79.98° vs Spot 1)	0.271 (78.59°) (211)

HRTEM analysis also disclosed the presence of some β-Zn$_4$Sb$_3$ regions, as indicated in Fig. 3. In addition, structural defects such as dislocations were also detected in the high magnification HRTEM image of ZnSb phase (as indicated in Fig. 3). These structural defects favor the phonon scattering and consequently decrease the thermal conductivity [24]. Both ZnSb and Zn$_4$Sb$_3$ phases exhibited polycrystalline nature with a high degree of crystallinity.

3.3 Thermoelectric properties

Figure 4 displays the temperature dependence of the electrical resistivity, Seebeck coefficient and power factor of Zn$_{1+x}$Sb (x=0, 0.05, 0.1, 15, 0.25, 0.3) samples. For pure ZnSb (x=0), the electrical resistivity slightly increased with temperature up to about 500 K, and then decreased with further increase in temperature. The measured electrical resistivity of ZnSb at room temperature was 86.54 $\mu\Omega\cdot$m, which was close to the value of ~66 $\mu\Omega\cdot$m reported by XIONG et al [25], but it was significantly lower than the value of 250 $\mu\Omega\cdot$m reported by VALSET et al [26] for ZnSb. This wide range of measured resistivities may be directly attributed to the different contents of β-Zn$_4$Sb$_3$ phase and its distribution within the ZnSb matrix [6]. The room temperature resistivity of Zn$_{1+x}$Sb samples continuously decreased with increasing Zn content, and reached the value of 21.47 $\mu\Omega\cdot$m for x=0.3, which was close to the typical reported resistivity of around 20 $\mu\Omega\cdot$m for β-Zn$_4$Sb$_3$ at room temperature [12]. Interestingly, all other samples exhibited an intermediate behavior between ZnSb and β-Zn$_4$Sb$_3$ phases. For 0≤x≤0.15, where ZnSb was the dominant phase in Zn$_{1+x}$Sb samples, the measured resistivities showed a similar trend to that of ZnSb, while for x>0.15, the measured resistivity trend resembled that of β-Zn$_4$Sb$_3$.

The Zn$_{1+x}$Sb materials exhibited the p-type conductivity in the entire temperature and compositional range of 0≤x≤0.3. The Seebeck coefficient decreased with increasing x in Zn$_{1+x}$Sb materials, following an identical trend as the electrical resistivity. The highest and the lowest Seebeck coefficients were measured from the nearly pure ZnSb and β-Zn$_4$Sb$_3$ samples in the entire temperature range of 300−650 K, respectively. The

Seebeck coefficient of Zn$_{1.3}$Sb increased from 124.5 μV/K at room temperature to 189.4 μV/K at near 650 K. The room temperature Seebeck coefficient of ZnSb was 286 μV/K and decreased to 258 μV/K at 650 K. The other materials exhibited a trend similar to ZnSb or β-Zn$_4$Sb$_3$ depending on the percentages of these two phases.
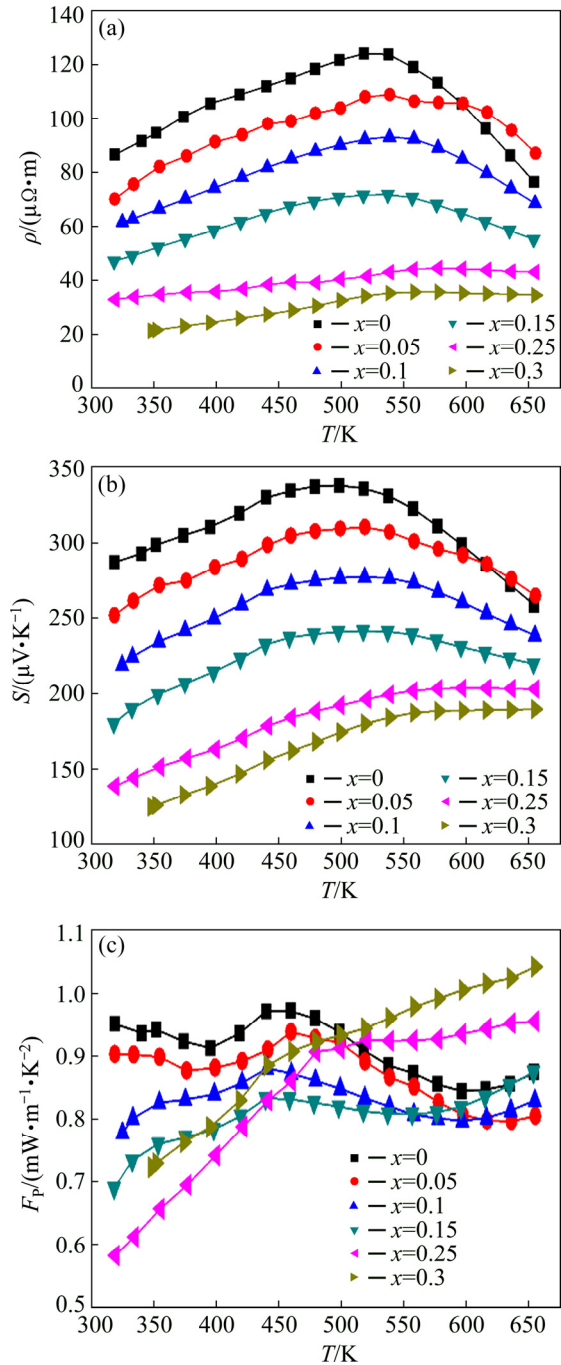

Fig. 4 Temperature dependence of electrical resistivity, ρ (a), Seebeck coefficient, S (b), and power factor, F_P (c), for Zn$_{1+x}$Sb samples, indicating decrease in electrical resistivity and Seebeck coefficient with increasing x in Zn$_{1+x}$Sb samples

The power factor (PF) of $Zn_{1+x}Sb$ materials also exhibited distinct behaviors in the compositional ranges of $0 \leq x \leq 0.15$ and $x > 0.15$. When $0 \leq x \leq 0.15$, an almost identical PF was obtained for all $Zn_{1+x}Sb$ samples in the entire temperature range measured, which was comparable to the typical behavior of nearly pure ZnSb [25]. Here, the PF of our ZnSb compound was about 0.95 $mW \cdot m^{-1} \cdot K^{-2}$ at room temperature, slightly fluctuated with increasing temperature and reached 0.87 $mW \cdot m^{-1} \cdot K^{-2}$ at 650 K. On the other hand, $Zn_{1.25}Sb$ and $Zn_{1.3}Sb$ samples possessed a relatively low PF at room temperature that significantly increased up to 0.95 and 1.04 $mW \cdot m^{-1} \cdot K^{-2}$ at temperatures around 650 K, respectively. These results suggested that the TE properties of $Zn_{1+x}Sb$ materials were a combination of the TE properties of ZnSb and β-Zn_4Sb_3 dominated by the phase with higher content.

The variation of total thermal conductivity κ with temperature for $Zn_{1+x}Sb$ samples is presented in Fig. 5. A relatively high thermal conductivity was observed for ZnSb over the entire temperature range measured. The stoichiometric ZnSb sample had a thermal conductivity of 1.81 $W \cdot m^{-1} \cdot K^{-1}$ at room temperature, while $Zn_{1.3}Sb$ (the nearly pure β-Zn_4Sb_3) showed a thermal conductivity of only 0.70 $W \cdot m^{-1} \cdot K^{-1}$ at room temperature. The measured thermal conductivities were in good agreement with the reported values for pure ZnSb [26] and β-Zn_4Sb_3 [27,28]. Thermal conductivity decreased with increasing temperature for all the samples.

Beside point defects and nanostructure features, the intrinsic structural and compositional distribution is a dominant factor determining thermal conductivity. In β-Zn_4Sb_3, the anharmonic motion of the Sb1 atoms coordinated only by Zn atoms results in ultralow thermal conductivities [11]. On the other hand, the simple crystal structure of ZnSb leads to a relatively high thermal conductivity. In $Zn_{1+x}Sb$ materials, the phase fraction of β-Zn_4Sb_3 significantly increased from 0 for ZnSb to 85.6% for $Zn_{1.3}Sb$ ($x=0.3$), as obtained from XRD results. The β-Zn_4Sb_3 content itself and indirectly the amount of ZnSb/β-Zn_4Sb_3 interfaces had a dominate effect on the lattice (κ_l) and electronic (κ_e) thermal conductivity. The lattice contribution and electronic contribution to thermal conductivity of the $Zn_{1+x}Sb$ materials are plotted in Fig. 6. The lattice conductivity (κ_l) was calculated by subtracting the electronic thermal conductivity (κ_e) from the measured thermal conductivity (κ_t). The electronic thermal conductivity was evaluated using the Wiedemann−Franz equation [24], and the Lorenz number was estimated from the measured Seebeck
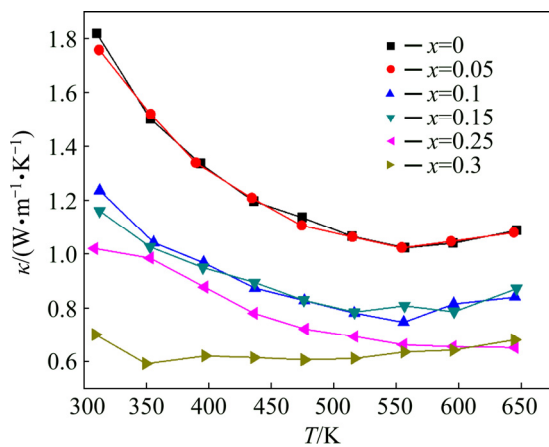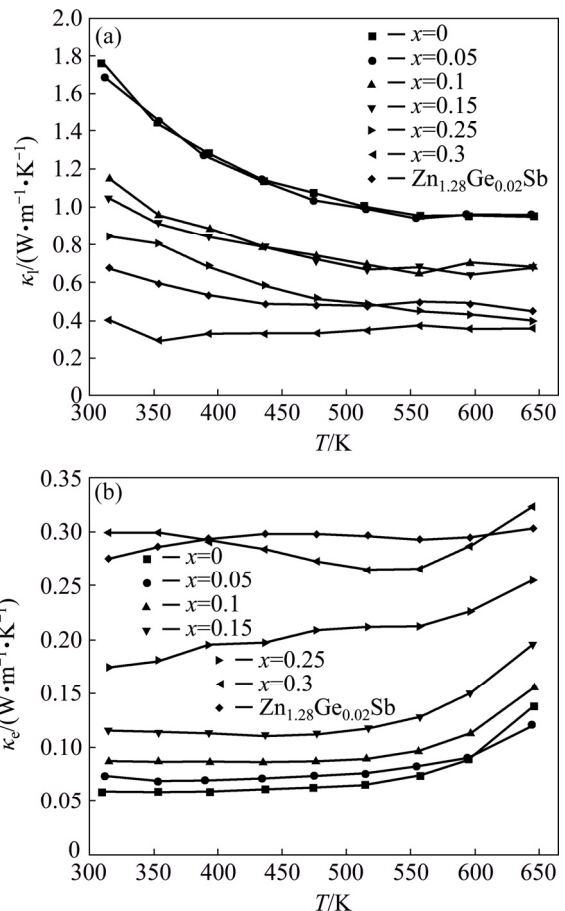

Fig. 5 Total thermal conductivities of $Zn_{1+x}Sb$ samples as function of temperature, exhibiting characteristic low thermal conductivity of β-Zn_4Sb_3 phase with increasing x in $Zn_{1+x}Sb$ samples

Fig. 6 lattice (a) and electronic (b) thermal conductivities of $Zn_{1+x}Sb$ compounds as function of temperature

coefficient [29]. A lattice thermal conductivity of $1.76 \, W \cdot m^{-1} \cdot K^{-1}$ was obtained for ZnSb at room temperature, which was almost four times higher than the value of $0.40 \, W \cdot m^{-1} \cdot K^{-1}$ obtained for $Zn_{1.3}Sb$ ($x=0.3$). The results indicated a substantial role for β-Zn_4Sb_3 content in the thermal conductivity of $Zn_{1+x}Sb$ materials.

Figure 7 displays the temperature dependence of thermoelectric figure of merit (Z_T) for $Zn_{1+x}Sb$ samples. The $Zn_{1.3}Sb$ sample exhibited the best TE performance in the entire temperature range of 300−650 K with a maximum Z_T value of 0.99 at 650 K, owing to its low thermal conductivity. The highest Z_T value obtained here for $Zn_{1.3}Sb$ was higher than that reported by ZOU et al [30] and WANG et al [31], but lower than that reported by LIN et al [12] and WANG et al [32] for pure β-Zn_4Sb_3. This can be mainly attributed to the presence of different contents of ZnSb in the synthesized materials. On the other hand, the maximum Z_T value of ZnSb was about 0.52 at 650 K, close to the reported values of 0.5 by VALSET et al [26] and 0.6 by POTHIN et al [16].
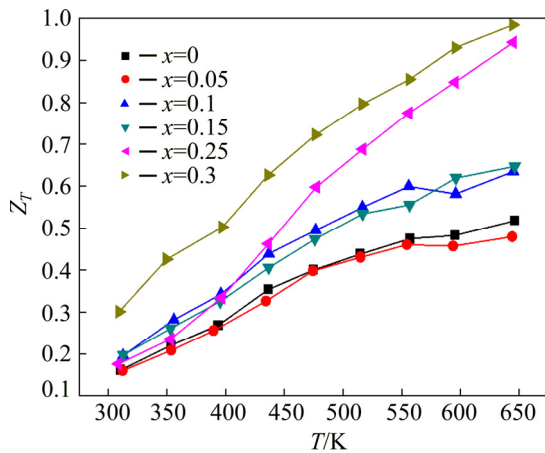

Fig. 7 Z_T values for $Zn_{1+x}Sb$ materials as function of temperature with $Zn_{1.3}Sb$ showing the best TE performance with maximum Z_T value of 0.99 at 650 K

To further optimize the TE properties of $Zn_{1+x}Sb$ materials, we partially substituted Ge for Zn in the $Zn_{1.3}Sb$ sample. Figure 8 shows the TE properties of Ge-substituted $Zn_{1.28}Ge_{0.02}Sb$ sample as a function of temperature. While the resistivity of $Zn_{1.28}Ge_{0.02}Sb$ sample was nearly identical to the resistivity of un-substituted $Zn_{1.3}Sb$ material, the Seebeck coefficient of Ge-substituted $Zn_{1.28}Ge_{0.02}Sb$ significantly increased in the entire temperature range measured. The maximum Seebeck coefficient

at 650 K increased from 189.4 µV/K for $Zn_{1.3}Sb$ to 220.7 µV/K for $Zn_{1.28}Ge_{0.02}Sb$. We tentatively ascribe the measured increase of Seebeck coefficient with the substitution of Ge to an increase in the density of state (DOS) near the Fermi level, which is indirectly associated with the modification of the electronic structure through introducing a narrow band of states in the valence band. This may result in a large increase in the effective mass and improvement of the Seebeck coefficient [32]. Consequently, the PF significantly increased in the entire temperature range measured (insert in Fig. 8(a)). The thermal conductivity of $Zn_{1.3}Sb$ also increased with the introduction of Ge. However, Ge substitution induced an large increase in Z_T because of the substantial boost in the power factor. A notable Z_T value of 1.17 was obtained for $Zn_{1.28}Ge_{0.02}Sb$ at 650 K. Besides, $Zn_{1.28}Ge_{0.02}Sb$ exhibited superior thermal stability than β-Zn_4Sb_3 materials synthesized by the conventional melting and quenching routes. Almost identical transport
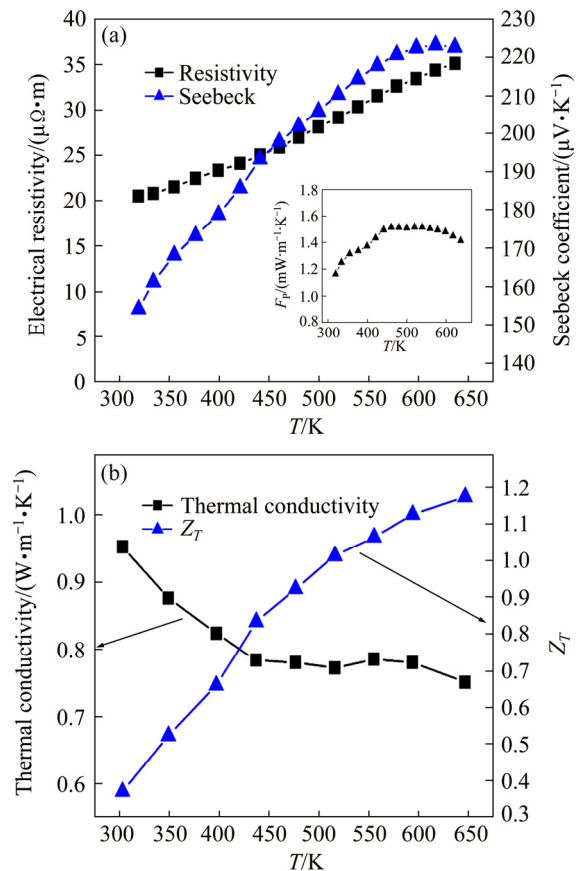

Fig. 8 Temperature dependence of electrical resistivity, Seebeck coefficient and power factor (insect) (a), and total thermal conductivities and Z_T values (b) of $Zn_{1.28}$-$Ge_{0.02}Sb$ as function of temperature with $Zn_{1.28}Ge_{0.02}Sb$ exhibiting notable Z_T value of 1.17 at 650 K

properties were recorded for $Zn_{1.28}Ge_{0.02}Sb$ during five cycles of repetitive measurements up to 650 K (Fig. 9). This superior stability may be attributed to the unique characteristics of our synthesis route including reaction in the solidus region of Zn−Sb binary phase diagram and cooling in a thermo-dynamically stable situation.
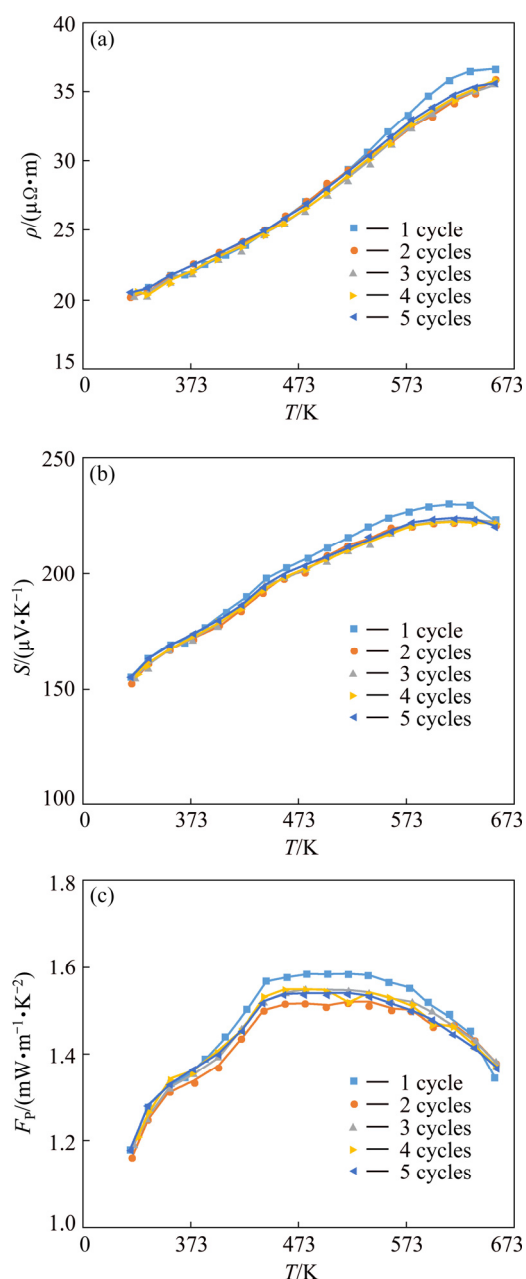

Fig. 9 Repetitive measurement of electrical transport properties of $Zn_{1.28}Ge_{0.02}Sb$ compound: (a) Electrical resistivity; (b) Seebeck coefficient; (c) Power factor

4 Conclusions

(1) Stable microstructures containing both ZnSb and β-Zn_4Sb_3 phases with no traces of Zn and Sb elements or new phases were obtained for all $Zn_{1+x}Sb$ samples with $x>0$.

(2) TE properties of all samples were a combination of the properties of ZnSb and β-Zn_4Sb_3 phases dominated by the phase with higher contents in the matrix.

(3) Ge substitution in $Zn_{1.3}Sb$ sample led to a substantial increase in the Seebeck coefficient concomitant to a nearly unchanged electrical resistivity, which considerably increased the power factor over the entire temperature range measured.

(4) A high Z_T value of 1.17 was obtained for $Zn_{1.28}Ge_{0.02}Sb$ at 650 K, which remained almost unchanged after five-cycle measurements.

References

[1] OSTOVARI MOGHADDAM A, SHOKUHFAR A, CABOT A, ZOLRIASATEIN A. Synthesis of bornite Cu_5FeS_4 nanoparticles via high energy ball milling: Photocatalytic and thermoelectric properties [J]. Powder Technology, 2018, 333: 160−166.

[2] ZHOU Shu-cai, BAI Chen-guang. Microwave direct synthesis and thermoelectric properties of Mg_2Si by solid-state reaction [J]. Transactions of Nonferrous Metals Society of China, 2011, 21(8): 1785−1789.

[3] OSTOVARI MOGHADDAM A, SHOKUHFAR A, CABOT A. Thermoelectric properties of nanostructured bornite $Cu_{5-x}Co_xFeS_4$ synthesized by high energy ball milling [J]. Journal of Alloys and Compounds, 2018, 750: 1−7.

[4] OSTOVARI MOGHADDAM A, SHOKUHFAR A, CABOT A. Ball milling and post annealing as an effective route to synthesize $Co_{1-x}Cu_xSbS$ paracostibite thermoelectric material [J]. Iranian Journal of Materials Science and Engineering, 2019, 16(4): 20−26.

[5] SHI Xiao-ya, WANG Li, CHEN Li-dong, CHEN Xi-hong. Thermoelectric properties of $M_xMo_6Te_8$ (M=Ag, Cu) [J]. Transactions of Nonferrous Metals Society of China, 2009, 19(3): 642−645.

[6] OSTOVARI MOGHADDAM A, SHOKUHFAR A, ZHANG Yu, ZHANG Ting, CADAVID D, ARBIOL J, CABOT A. Ge-doped ZnSb/β−Zn_4Sb_3 nanocomposites with high thermoelectric performance [J]. Advanced Materials Interfaces, 2019, 6(18): 1900467.

[7] MOZHARIVSKYJ Y, JANSSEN Y, HARRINGA J L, KRACHER A, TSOKOL A O, MILLER G J. $Zn_{13}Sb_{10}$: A structural and landau theoretical analysis of its phase transitions [J]. Chemistry of Materials, 2006, 18(3): 822−831.

[8] SNYDER G J, CHRISTENSEN M, NISHIBORI E, CAILLAT T, IVERSEN B B. Disordered zinc in Zn_4Sb_3 with phonon−glass and electron−crystal thermoelectric properties [J]. Nature Materials, 2004, 3(7): 458−463.

[9] PEDERSEN B L, IVERSEN B B. Thermally stable

thermoelectric Zn_4Sb_3 by zone-melting synthesis [J]. Applied Physics Letters, 2008, 92(16): 161907.

[10] YIN Hao, CHRISTENSEN M, LOCK N, IVERSEN B B. Zn migration during spark plasma sintering of thermoelectric Zn_4Sb_3 [J]. Applied Physics Letters, 2012, 101(4): 043901.

[11] SCHLECHT S, ERK C, YOSEF M. Nanoscale zinc antimonides: Synthesis and phase stability [J]. Inorganic Chemistry, 2006, 45(4): 1693−1697.

[12] LIN Jian-ping, LI Xu-dong, QIAO Guan-jun, WANG Zhao, CARRETE J, REN Yang, MA Ling-zhi, FEI You-jian, YANG Bai-feng, LEI Lei. Unexpected high-temperature stability of β-Zn_4Sb_3 opens the door to enhanced thermoelectric performance [J]. Journal of the American Chemical Society, 2014, 136(4): 1497−1504.

[13] FEDOROV M I, PROKOF'EVA L V, PSHENAY-SEVERIN D A, SHABALDIN A A, KONSTANTINOV P P. New interest in intermetallic compound ZnSb [J]. Journal of Electronic Materials, 2014, 43(6): 2314−2319.

[14] OKAMURA C, UEDA T, HASEZAKI K. Preparation of single-phase ZnSb thermoelectric materials using a mechanical grinding process [J]. Materials Transactions, 2010, 51(5): 860−862.

[15] POTHIN R, AYRAL R M, BERCHE A, ROUESSAC F, JUND P. Interest of the differential thermal analysis on the characterization of a thermoelectric material: ZnSb [J]. Journal of Alloys and Compounds, 2016, 657: 358−365.

[16] POTHIN R, AYRAL R M, BERCHE A, GRANIER D, ROUESSAC F, JUND P. Preparation and properties of ZnSb thermoelectric material through mechanical-alloying and spark plasma sintering [J]. Chemical Engineering Journal, 2016, 299: 126−134.

[17] LO CHUN-WAN T, SVITLYK V, CHERNYSHOV D, MOZHARIVSKYJ Y. The updated Zn−Sb phase diagram: How to make pure $Zn_{13}Sb_{10}$ ("Zn_4Sb_3") [J]. Dalton Transactions, 2018, 47(33): 11512−11520.

[18] TOBY B H, von DREELE R B. GSAS-II: The genesis of a modern open-source all purpose crystallography software package [J]. Journal of Applied Crystallography, 2013, 46(2): 544−549.

[19] RAUWEL P, LØVVIK O M, RAUWEL E, TAFTØ J. Nanovoids in thermoelectric β-Zn_4Sb_3: A possibility for nanoengineering via Zn diffusion [J]. Acta materialia, 2011, 59(13): 5266−5275.

[20] BALASUBRAMANIAN P, BATTABYAL M, SIVAPRAHASAM D, GOPALAN R. On the formation of phases and their influence on the thermal stability and thermoelectric properties of nanostructured zinc antimonide [J]. Journal of Physics D: Applied Physics, 2016, 50(1): 015602.

[21] ZHANG L T, TSUTSUI M, ITO K, YAMAGUCHI M. Effects of ZnSb and Zn inclusions on the thermoelectric properties of β-Zn_4Sb_3 [J]. Journal of Alloys and Compounds, 2003, 358(1−2): 252−256.

[22] FISCHER A, SCHEIDT E W, SCHERER W, BENSON D E, WU Y, EKLÖF D, HÄUSSERMANN U. Thermal and vibrational properties of thermoelectric ZnSb: Exploring the origin of low thermal conductivity [J]. Physical Review B, 2015, 91(22): 224309.

[23] NIEDZIOLKA K, POTHIN R, ROUESSAC F, AYRAL R M, JUND P. Theoretical and experimental search for ZnSb-based thermoelectric materials [J]. Journal of Physics: Condensed Matter, 2014, 26(36): 365401.

[24] OSTOVARI MOGHADDAM A, SHOKUHFAR A, GUARDIA P, ZHANG Yu, CABOT A. Substantial role of doping in the thermoelectric and hardness properties of nanostructured bornite, Cu_5FeS_4 [J]. Journal of Alloys and Compounds, 2019, 773: 1064−1074.

[25] XIONG Ding-bang, OKAMOTO N L, INUI H. Enhanced thermoelectric figure of merit in p-type Ag-doped ZnSb nanostructured with Ag_3Sb [J]. Scripta Materialia, 2013, 69(5): 397−400.

[26] VALSET K, BÖTTGER P H M, TAFTØ J, FINSTAD T G. Thermoelectric properties of Cu doped ZnSb containing Zn_3P_2 particles [J]. Journal of Applied Physics, 2012, 111(2): 023703.

[27] SONG Min-seok, CHOI Soon-mok, SEO Won-seon, MOON Jooho, JANG Kyung-wook. Thermoelectric and mechanical properties of Zn_4Sb_3 polycrystals sintered by spark plasma sintering [J]. Journal of the Korean Physical Society, 2012, 60(10): 1735−1740.

[28] DASGUPTA T, STIEWE C, SESSELMANN A, YIN H, IVERSEN B B, MUELLER E. Thermoelectric studies in β-Zn_4Sb_3—The complex interdependence between thermal stability, thermoelectric transport, and zinc content [J]. Journal of Applied Physics, 2013, 113(10): 103708.

[29] KIM H S, GIBBS Z M, TANG Y, WANG H, SNYDER G J. Characterization of Lorenz number with Seebeck coefficient measurement [J]. APL Materials, 2015, 3: 041506.

[30] ZOU Tian-hua, QIN Xiao-ying, ZHANG Yong-sheng, LI Xiao-guang, ZENG Zhi, LI Di, ZHANG Jian, XIN Hong-xing, XIE Wen-jie, WEIDENKAFF A. Enhanced thermoelectric performance of β-Zn_4Sb_3 based nanocomposites through combined effects of density of states resonance and carrier energy filtering [J]. Scientific Reports, 2015, 5: 17803.

[31] WANG Q Q, QIN X Y, LI D, ZOU T H. Enhancement of thermopower and thermoelectric performance through resonant distortion of electronic density of states of β-Zn_4Sb_3 doped with Sm [J]. Applied Physics Letters, 2013, 102(15): 154101.

[32] WANG Shan-yu, TAN Xiao-jian, TAN Gang-jian, SHE Xiao-yu, LIU Wei, LI Han, LIU Hui-jun, TANG Xin-feng. The realization of a high thermoelectric figure of merit in Ge-substituted β-Zn_4Sb_3 through band structure modification [J]. Journal of Materials Chemistry, 2012, 22(28): 13977−13985.

Zn$_{1+x}$Sb 二元体系的相形成和热电性能

Ahmad OSTOVARI MOGHADDAM[1], Evgeny TROFIMOV[1], Ting ZHANG[2], Jordi ARBIOL[2], Andreu CABOT[3,4]

1. Department of Materials Science, Physical and Chemical Properties of Materials,

South Ural State University, 76 Lenin Ave, Chelyabinsk, 454080, Russia;

2. Catalan Institute of Nanoscience and Nanotechnology (ICN2),

Consejo Superior de Investigaciones Científicas (CSIC) and Barcelona Institute of Science and Technology (BIST),

Campus Autonomous University of Barcelona (UAB), Bellaterra, 08193 Barcelona, Spain;

3. Catalonia Institute for Energy Research-IREC, Sant Adrià de Besòs, 08930 Barcelona, Spain;

4. Catalan Institution for Research and Advanced Studies-ICREA, Pg. Lluís Companys 23, 08010 Barcelona, Spain

摘　要：在 Zn−Sb 二元相图固相线以下使 Zn 和 Sb 粉末反应并随炉冷却，合成一系列 Zn$_{1+x}$Sb (x=0, 0.05, 0.1, 0.15, 0.25, 0.3) 材料，分析 Zn–Sb 相图中心区域的相形成和热电性能。在此过程中，非化学计量比的混合粉末结晶形成 ZnSb 和 β-Zn$_4$Sb$_3$ 相的组合。然后，将材料研磨并热压成致密的 ZnSb/β-Zn$_4$Sb$_3$ 复合材料。X 射线衍射、高分辨率透射电镜和电子能量损失谱分析均未发现 Sb、Zn 元素或其他相。所有材料的热电性能都可以归结为 ZnSb 和 β-Zn$_4$Sb$_3$ 相的热电行为的结合，并由每种材料中的主相所决定，Zn$_{1.3}$Sb 复合材料具有最好的热电性能。研究发现，Ge 掺杂可大幅增加 Zn$_{1.3}$Sb 的 Seebeck 系数且显著提高其功率因数，540 K 时达 1.51 mW·m^{-1}·K^{-2}。 总之，Zn$_{1.28}$Ge$_{0.02}$Sb 具有优异、稳定的 Z_T 值，650 K 时为 1.17。

关键词：Zn$_{1+x}$Sb；ZnSb/β-Zn$_4$Sb$_3$ 复合材料；热稳定性；热电性能

(Edited by Bing YANG)